

Superwind-Driven Intense H₂ Emission in NGC 6240

Youichi OHYAMA,¹ Michitoshi YOSHIDA,² Tadafumi TAKATA,³ Masatoshi IMANISHI,^{1,4}
 Tomonori USUDA,³ Yoshihiko SAITO,⁵ Hiroko TAGUCHI,⁶ Noboru EBIZUKA,⁷
 Fumihide IWAMURO,⁸ Kentaro MOTOHARA,⁸ Tomoyuki TAGUCHI,⁸ Ryuji HATA,⁸
 Toshinori MAIHARA,⁹ Masanori IYE,¹ Toshiyuki SASAKI,³ George KOSUGI,³
 Ryusuke OGASAWARA,³ Junichi NOUMARU,³ Yoshihiko MIZUMOTO,¹ Masafumi YAGI,¹
 and Yoshihiro CHIKADA¹

¹ National Astronomical Observatory of Japan, 2-21-1 Osawa, Mitaka, Tokyo 181-8588

E-mail(YO): *ohyama@optik.mtk.nao.ac.jp*

² Okayama Astrophysical Observatory, NAOJ, Kamogata-cho, Okayama 719-0232

³ Subaru Telescope, NAOJ, 650 A'ohoku Place, Hilo, HI 96720, USA

⁴ Institute for Astronomy, University of Hawaii, Honolulu, HI 96822, USA

⁵ Department of Astronomy, University of Tokyo, Bunkyo-ku, Tokyo 113-0033

⁶ Department of Astronomy and Earth Sciences, Tokyo Gakugei University, Koganei, Tokyo 184-8501

⁷ Communications Research Laboratory, Koganei, Tokyo 184-8795

⁸ Department of Physics, Kyoto University, Sakyo-ku, Kyoto 606-8502

⁹ Department of Astronomy, Kyoto University, Sakyo-ku, Kyoto 606-8502

(Received 1999 December 22; accepted 2000 January 14)

Abstract

We have performed a long-slit K band spectroscopic observation of the luminous infrared galaxy NGC 6240. Spatially extended H₂ emission is detected over 3.3 kpc around the two nuclei. The peak position of the H₂ $v = 1 - 0$ $S(1)$ emission in the slit is located $\sim 0.^{\prime\prime}3 - 0.^{\prime\prime}4$ north of the southern nucleus. It is almost the midpoint between the southern nucleus and the peak position of the ¹²CO ($J = 1 - 0$) emission. Based on the line-ratio analyses, we suggest the excitation mechanism of H₂ is pure thermal at

most positions. In the northern region including the northern nucleus, the H₂ velocity field shows only a slight velocity gradient and is not highly disturbed. On the other hand, the kinematics of the H₂ emitting gas is more complicated around the southern nucleus and its south region. In the southern region we find the following three velocity components in the H₂ emission: the blueshifted shell component (≈ -250 km s⁻¹ with respect to V_{sys}) which is recognized as a distinct C-shape distortion in the velocity field around the southern nucleus, the high-velocity blueshifted “wing” component (~ -1000 km s⁻¹ with respect to V_{sys}), and the component indicating possible line splitting of ~ 500 km s⁻¹. The latter two components are extended to the south from the southern nucleus. We show that the kinematic properties of these three components can be reproduced by expanding motion of a shell-like structure around the southern nucleus. The offset peak position of the H₂ emission can be understood if we assume that the shell expanding to the north interacts with the extragalactic molecular gas which has been transferred during the course of the merging of the two nuclei. At the interface between the shell and the molecular gas concentration the cloud-crushing mechanism proposed by Cowie et al. (1981) may work efficiently, and the intense H₂ emission is thus expected there. With this mechanism, the H₂ luminosity can be explained without global shock driven by the collision of the two nuclei. All these findings lead us to propose a model that the most H₂ emission is attributed to the shock excitation driven by the superwind activity of the southern nucleus.

Key words: Infrared: galaxies — Infrared: spectra — Galaxies: individual (NGC 6240) — Galaxies: interacting — Galaxies: intergalactic medium — Shock waves

1. Introduction

NGC 6240 (= IRAS 16504+0228 = UGC 10592 = IC 4625) is one of the famous luminous infrared galaxies (LIGs: $L(\text{IR}) = L(8 - 1000\mu\text{m}) = 4.6 \times 10^{11} L_{\odot}$: Sanders & Mirabel 1996) at a distance of 98 Mpc (Heckman et al. 1987). It is a merging system containing two radio and near-infrared nuclei (Condon et al. 1982; Fried & Schulz 1983; Eales et al. 1990; Thronson et al. 1990; Herbst et al. 1990; Colbert, Wilson, & Bland-Hawthorn 1994; Sugai et al. 1997; Tacconi et al. 1999). Although this galaxy is often called as a prototypical LIG (Wright, Joseph, & Meikle 1984; Joseph & Wright 1984; Heckman, Armus, & Miley 1987, 1990; Armus, Heckman, & Miley 1990; Klaas et al. 1997), it is also well known as an object with unusually luminous near-infrared molecular hydrogen (H₂) emission

(e.g., Rieke et al. 1985; DePoy, Becklin, & Wynn-Williams 1986). Several H₂ excitation mechanisms have been proposed to date including 1) thermal excitation driven by shocks (Rieke et al. 1985; DePoy et al. 1986; Lester, Harvey, & Carr 1988; Elston & Maloney 1990; Herbst et al. 1990; van der Werf et al. 1993; Sugai et al. 1997), 2) UV fluorescence (Tanaka, Hasegawa, & Gatley 1991), 3) soft X-ray heating (Draine & Woods 1990; see also Mouri et al. 1989), and 4) formation pumping (Mouri & Taniguchi 1995). Recently, Sugai et al. (1997) presented their new high-quality spectrum and clearly showed that the H₂ spectrum can be interpreted as a pure thermal excitation. Although the origin of the H₂ emission in LIGs and ultraluminous infrared galaxies (ULIGs: Sanders & Mirabel 1996) is generally attributed to their intense star-formation activities at their nuclei and/or active galactic nuclei (AGNs) (e.g., Moorwood & Oliva 1990; Goldader et al. 1995), NGC 6240 is often considered to be an exceptional case. It is often discussed that the global shock caused by a galaxy-galaxy collision brings its huge H₂ luminosity. This is because 1) current star-formation activity (or, current supernova explosion rate) is not intense enough to reproduce its huge H₂ luminosity (e.g., Rieke et al. 1985; Draine & Woods 1993), 2) unusually large intensity ratio of H₂ $v = 1 - 0$ $S(1)$ [hereafter, $1 - 0$ $S(1)$] to Br γ ($\simeq 45$: van der Werf et al. 1990) cannot be explained by normal star-formation activities (e.g., Rieke et al. 1985; Draine & Woods 1993), and 3) the peak position of the H₂ emission is located not at each nucleus but between the two nuclei where no star-forming activity is detected (Herbst et al. 1990; van der Werf et al. 1993; Sugai et al. 1997). However, it is important to remember that these kinds of evidence are not direct ones, i.e., we do not have any spatial and kinematic information directly suggesting that the intense H₂ emission does come from the galaxy-galaxy collision interface.

Although thermal excitation driven by the galaxy-galaxy collision might be a main excitation mechanism of the strong H₂ emission, there remains some possibilities of other excitation mechanisms. Like other normal LIGs, it seems very likely that intense starburst activity and/or AGN also contribute more or less to the H₂ emission. In fact, there are many pieces of evidence suggesting intense starburst activity in this galaxy (Wright et al. 1984; Rieke et al. 1985; Smith, Aitken & Roche 1989; van der Werf et al. 1993). Also there are many pieces of evidence suggesting an activity of “superwind”, which is a galaxy scale blastwave driven by numerous supernova explosions (Tomisaka & Ikeuchi 1989; Heckman et al. 1990; Suchkov et al. 1994), and some previous authors have indeed suggested its importance to the H₂ emission (Elston & Maloney 1990; Herbst et al. 1990; van der Werf et al. 1993). X-ray heating from an AGN, which is recently found by the hard X-ray observation (Iwasawa & Comastri 1998), might also contribute to the H₂ emission (Mouri et al. 1989). In this way, the physical mechanism of the H₂ emission seems

to be very complicated in this galaxy.

In order to study the origin of the H₂ emission in more detail and to understand the nature of the activity of NGC 6240, it is important to obtain a spatial information of the emission-line properties. Thus, we have conducted a long-slit K-band spectroscopic observations of this galaxy with Subaru 8.2m telescope (Kaifu 1998) in order to perform detailed spectroscopic analyses.

2. Observation and Data Reduction

Observations were performed on the night of 1999 April 29 during the test observation phase of Subaru telescope at the top of Mauna Kea, Hawaii, using the grism spectroscopy mode of CISCO (Cooled Infrared Spectrograph and Camera for OHS: Motohara et al. 1998). The detector used is a 1024×1024 Hawaii array with a projected pixel size of $0.^{\prime\prime}115$ along the slit and 8.6\AA at $2.3\mu\text{m}$ along the dispersion direction. Slit width is $0.^{\prime\prime}5$ and slit length is about 2 arcminutes, which is long enough to obtain sky background information in each on-source frame. The slit position angle was set to the position angle of the two nuclei (19° : Herbst et al. 1990; Thronson et al. 1990) in order to observe the northern and southern nuclei (hereafter, the N nucleus and the S nucleus, respectively) as well as the intergalactic region at a same time (Figure 1¹).

The total exposure time was 1500 second for on source (fifteen exposures, each of 100 second integration). The object was placed on only two positions along the slit during exposures. A nearby A3-type star SAO 122007 and a K0-type star SAO 122106 were also observed just before observing NGC 6240 in order to correct for atmospheric absorption. Seeing size around K band wavelength were $0.^{\prime\prime}5 - 0.^{\prime\prime}6$ during the observations. Dome flat spectra were obtained at another observing run on 1999 June 25 with the same instrumental setup.

Data reduction was performed with IRAF². First, the dark is subtracted from each frame. Each dark-subtracted frame was divided by the dark-subtracted dome flat spectrum. Then, wavelength calibration of each frame was made using the telluric OH emission lines to an accuracy of $\sim 2.6\text{\AA}$. The spectral resolution measured from the OH

1 This image was obtained with the CISCO imaging mode with a K band filter through a wide $2.^{\prime\prime}$ slit with the position angle of 19° .

Note that because this image was taken just for the source acquisition, the dark subtraction and the flatfielding were not applied. It is presented just for the reader to easily understand the rough source positions along the slit. The image is averaged over 2 pixels ($0.^{\prime\prime}23$).

2 IRAF is distributed by the National Optical Astronomy Observatories, which are operated by the Association of Universities for Research in Astronomy, Inc., under cooperative agreement with the National Science Foundation.

emission lines was $\sim 26\text{\AA}$ FWHM at $2.2\mu\text{m}$ (350 km s^{-1}). We have measured the wavelength of the OH lines in the wavelength-calibrated sky spectra and found that the systematic error is less than 1\AA around $2.2\mu\text{m}$ (14 km s^{-1}). Background sky emission was removed by interpolating the adjacent sky spectra with a linear interpolation. The wavelength calibrated frames were combined using 3σ clipping averaging method after shifting the images along the slit. The spectra of the standard stars were also reduced in the same way. Br γ absorption feature of the A-type star was removed in the following way. First, the spectrum of the A-type star was divided by that of the K-type star in order to cancel out the common features such as the atmospheric absorption and the instrumental sensitivity. The resultant ratio spectrum shows an isolated Br γ absorption feature and this feature was removed using Voigt profile fitting. Then, the ratio spectrum was multiplied by the spectrum of the K-type stars, giving modified A-type star spectrum without Br γ absorption feature. The modified spectrum was used for correcting the atmospheric absorption features and instrumental sensitivity assuming a 8590 K blackbody spectrum. Because the sky condition was not photometric during the observations, no absolute flux calibration was made.

3. Results

3.1. Broadband image

Broad K band image (Figure 1) clearly shows two nuclei (the N and the S nuclei) at a separation of $\simeq 1.^{\prime\prime}9$ with the position angle of $\simeq 19^\circ$. This result is consistent with the previous studies in K band (Eales et al. 1990; Herbst et al. 1990; Thronson et al. 1990; Sugai et al. 1997), although Herbst et al. (1990) reported a slightly smaller separation of the two nuclei ($1.^{\prime\prime}52 \pm 0.^{\prime\prime}02$).

One must be careful when comparing the nuclear positions seen in the radio continuum and the K band image. Colbert et al. (1994) and Tacconi et al. (1999) found the double nuclei in the radio continuum emission. Although the position angles of the two radio nuclei (19.7 and 21° at 8.3 GHz and 5 GHz , respectively) are consistent with one of the K band nuclei (19°), the distance between the two is significantly smaller in radio ($\simeq 1.^{\prime\prime}53$ and $1.^{\prime\prime}7$ at 8.3 GHz and 5 GHz , respectively) than in K band ($\sim 1.^{\prime\prime}9$). This apparent discrepancy can be understood as an effect of the dust extinction. The visual extinction (A_v) of this galaxy inferred from the large column density ($N_{\text{H}_2} \gtrsim 2 \times 10^{23} \text{ cm}^{-2}$) is as large as $\gtrsim 200$ mag (Tacconi et al. 1999), indicating heavy dust extinction even at K band ($A_k \simeq 0.112 \times A_v \gtrsim 22$ mag; Binney & Merrifield 1998). Thus the true nuclei should be at the extinction-free

radio nuclei, i.e., the true N and S nuclei are located at slightly south and north of the apparent K band positions ($\sim 0.^{\prime\prime}1 - 0.^{\prime\prime}2$), respectively.

3.2. The spectra and the flux distribution

Spatially extended H₂ emission is detected over 7'' region (3.3 kpc) around the two nuclei. Figure 2 shows the K band spectra of NGC 6240 at various positions. Rich H₂ line features including 1 - 0 S(0), 1 - 0 S(1), 1 - 0 S(2), 1 - 0 S(3), 2 - 1 S(1), and 2 - 1 S(3) emission lines are detected at most positions. The 2 - 1 S(2) and possibly 2 - 1 S(4) lines are also detected at some positions. Weak Br γ emission is detected at both the N and the S nuclei. Deep stellar CO absorption is also detected at both nuclei, being consistent with the report by Lester & Gaffney (1994).

The peak position of 1 - 0 S(1) is located at about 0.^{\prime\prime}3 - 0.^{\prime\prime}4 north-north-east of the S nucleus (Figure 3) and is much closer to the S nucleus than to the N nucleus. Recent high resolution ¹²CO($J = 2 - 1$) mapping shows that the CO peak position is located at 0.^{\prime\prime}6 north-north-east of the S nucleus seen in the radio continuum images (Tacconi et al. 1999) and is marked in Figure 1. Thus, the peak position of 1 - 0 S(1) is located at almost the midpoint between the CO peak position and the S nucleus. This result is inconsistent with the previous works based on narrow-band emission-line imagings, showing that intense 1 - 0 S(1) emission arises from the region between two nuclei with its peak around the midpoint of the two (Herbst et al. 1990; van der Werf et al. 1993; Sugai et al. 1997). Note, however, that the overall spatial extent of the H₂ emission found in our data is nearly consistent with the previous results. The equivalent width of the 1 - 0 S(1) emission is the lowest (20 - 40Å) at both nuclei, where the continuum emission is the strongest, and is larger at other regions ($\gtrsim 100\text{\AA}$).

3.3. The velocity field

The heliocentric velocities and the line widths of the 1 - 0 S(1) emission measured with a single Gaussian fitting at various positions are shown in Figure 3. A continuum-subtracted peak-normalized 1 - 0 S(1) spectroscopic image is also shown in Figure 4. The velocity is nearly constant and is approximately 7300 km s⁻¹ in the northern region including the N nucleus and its north. We find the systemic velocity V_{sys} of NGC 6240 $\simeq 7300$ km s⁻¹ from compilation of the previously published infrared and radio observations (the previous measurements of V_{sys} are summarized in Table 1.). Thus, the radial velocity of the H₂ emitting gas coincides with the systemic one and the

gas motion is relatively quiescent in the northern region.

On the other hand, we find a remarkable velocity variation in the southern region: the emission line is significantly blueshifted and the velocity field is highly disturbed to form a C-shaped distortion over $\sim 1''$ (450 pc) region around the S nucleus (see Figure 4). At $0.''3 - 0.''5$ south from the S nucleus the velocity reaches down to -250 km s^{-1} ($V_\bullet \simeq 7050 \text{ km s}^{-1}$; see Figure 3) with respect to V_{sys} . It must be remembered that the true position of the S nucleus after correcting for the extinction between the two nuclei is expected to be located about $\sim 0.''1 - 0.''2$ north of the

apparent K band nucleus. Thus, the center of the C-shaped distortion almost corresponds spatially to the true S nuclear position. It is noteworthy that about 50% of the $1 - 0$ $S(1)$ emission covered in our slit comes from this blueshifted region. This kind of a peculiar velocity field has been previously found by Elston & Maloney (1990), but they could not resolve the detailed structure of the velocity field because of the limited spatial and velocity resolution of their spectrum. We first revealed the detailed dynamical structure of the circumnuclear H_2 emission-line region of NGC 6240.

This remarkable C-shaped velocity field would account for the difference between the flux peak position of $1 - 0$ $S(1)$ measured by this work and that derived from the previous narrow band imagings. As pointed out in the previous section, we find that the peak position of $1 - 0$ $S(1)$ is located much closer to the S nucleus than previously reported positions. How can we understand this difference? Using narrow band imagings, Sugai et al. (1997) showed that the peak of $1 - 0$ $S(1)$ is located between the two nuclei. Their images were taken with three Fabry-Perot settings at V_{sys} (7339 km s^{-1} in their paper), $V_{\text{sys}} - 175 \text{ km s}^{-1}$, and $V_{\text{sys}} + 175 \text{ km s}^{-1}$. Comparing with our results, it seems likely that the most blueshifted $1 - 0$ $S(1)$ emission ($\sim 7000 - 7100 \text{ km s}^{-1}$) could not be detected in their images. Based on their three narrow-band images (centered at $V_\bullet = 6910, 7390$, and 7470 km s^{-1}), van der Werf et al. (1993) showed that the position of the $1 - 0$ $S(1)$ peak moves from south to north with increasing velocity, although the peak position of the velocity-integrated $1 - 0$ $S(1)$ emission comes around the midpoint of the two nuclei. The blueshifted $1 - 0$ $S(1)$ emission found in our data ($V_{\text{sys}} - 250 \text{ km s}^{-1}$) should be detected in their blue-band image in which the peak is closer to the S nucleus, being consistent with our result. Herbst et al. (1990) found a southwest extension of the $1 - 0$ $S(1)$ emission ($\lesssim 0.''5$ from the S nucleus) in addition to the component around the midpoint of the two nuclei³. Since our slit position angle is 19° , it seems likely that our slit covers a part of this extension.

³ Although Sugai et al. (1997) emphasized that the peak position of the $1 - 0$ $S(1)$ emission is located between the two nuclei, we

If this component is blueshifted with respect to V_{sys} , then it would be observed as a blueshifted component around the S nucleus in our data. In these ways, we find that our result is consistent with the previous results.

In addition to the blueshifted emission around the S nucleus, we find a high-velocity blueshifted emission-line “wing” whose velocity exceeds -1000 km s^{-1} with respect to the peak velocity of the profile (Figure 4). This kind of a profile was previously found by van der Werf et al. (1993). With our spatially resolved spectra, we can investigate the spatial distribution of this high-velocity wing component and find that such a component extends around the S nucleus and to its southern regions ($\sim 2''$, or $\sim 950 \text{ pc}$).

The line width is nearly constant at the region between the two nuclei and around the N nucleus ($550 - 600 \text{ km s}^{-1}$ FWHM after correcting for the instrumental line broadening), which is consistent with the previous results (e.g., van der Werf et al. 1993). It is well known that this galaxy shows unusually broader line width ($\simeq 550 \text{ km s}^{-1}$) compared with other galaxies with the intense H_2 emission (e.g., van der Werf et al. 1993). We newly find that the line width at $1'' - 2''$ south of the S nucleus is even broader ($700 - 800 \text{ km s}^{-1}$ FWHM) than more northern regions⁴. We also find that the line profile at this region shows boxy profile (with nearly flat-topped profile and relatively weak low intensity wing) rather than an usual Gaussian-like profile seen in more northern regions (Figure 4). In order to understand this peculiar line profile, we try to represent the observed spectra with the combination of two velocity components each of which is blue- and redshifted with respect to the mean central velocity measured with the single Gaussian fitting (Figure 3). We assume Gaussian line profile with the line width of 550 km s^{-1} FWHM for each component. For simplicity, the intensities of the two components are set to be equal because of the nearly symmetric line profile (except for the low intensity blueshifted high-velocity wing component). The central velocity is set to $V_{\text{sys}} - 100 \text{ km s}^{-1}$ from Figure 3. The fitting was made by eye. As a result, we find that superposition of the two components with a velocity difference of 500 km s^{-1} can represent the observed line profile at $7''$ south of the S nucleus (Figure 5). We thus propose a model that two broad (550 km s^{-1} FWHM) emission lines whose velocity difference is $\approx 500 \text{ km s}^{-1}$ make the boxy profile seen in the southern region. Note that the velocity difference of the two components (500 km s^{-1}) is nearly twice the velocity of the C-shaped velocity distortion observed around the S nucleus (250 km s^{-1}).

point out that their contour plot also shows an extension toward the southwest direction (see their Figure 1). This extension seems to correspond to the southwest extension found in Herbst et al. (1990).

⁴ A reason why previous studies reported relatively narrow line width may be that the line width tends to be narrower at stronger H_2 emission region and that they could only measure the intensity-weighted line width because of their insufficient spatial resolution.

The line width of the $\text{Br}\gamma$ emission is nearly the same as that of the $1 - 0 S(1)$ emission (i.e., $\sim 500 - 600 \text{ km s}^{-1}$ FWHM) at all positions with a detectable $\text{Br}\gamma$ emission. We find no kinematic evidence for the presence of a broad line region of AGN ($\gtrsim 5000 \text{ km s}^{-1}$ FWHM; Osterbrock 1989).

3.4. Emission-line ratios and the excitation mechanism

We examine the H_2 excitation mechanism at various positions. Following Mouri (1994), we show a line-ratio diagnostic diagram for discussing the excitation mechanisms in Figure 6. Some data points scatter around a theoretical locus of the thermal excitation with a temperature of about 2000 K. Others show slightly lower $1 - 0 S(2)/1 - 0 S(0)$ ratio and scatter around observed data points of supernova remnants (SNRs). It is known that temperature gradient within the shock front causes the ratio slightly lower than this locus in SNRs (e.g., Beckwith et al. 1983). Thus, the molecular gas is thermally excited at most positions. On the other hand, we find no evidence for the non-thermal excitation with the larger $2 - 1 S(1)/1 - 0 S(1)$ ratio ($\gtrsim 0.5$) anywhere.

We also show population diagrams at various positions (Figure 7). We find that the data points at each position are aligned along a single straight line on this diagram, indicating that thermal excitation is dominated at most positions. The region at $1'' - 1.''2$ south of the S nucleus marginally shows relatively stronger $1 - 0 S(1)$ and weaker $2 - 1 S(3)$ emissions. Figure 8 shows a spatial variation of the $v = 2 - 1$ vibration temperature (T_{vib}) and $v = 1$ rotation temperature (T_{rot}). Most regions show a temperature of $\sim 2000 \text{ K}$, being consistent with the results of Sugai et al. (1997). In order to assess a possible contribution of other excitation mechanisms, we show a plot of the ratio of T_{vib} to T_{rot} as a function of slit positions (Figure 8). The ratio should be unity in case of a pure thermal excitation and be slightly larger in shocks with a temperature gradient (which is empirically $\simeq 1.25 = 1/0.8$; Tanaka et al. 1991). In case of an UV fluorescent, the ratio becomes much larger than unity since T_{vib} ($\sim 6000 \text{ K}$) is much larger than T_{rot} ($\sim 1000 \text{ K}$) (e.g., Tanaka et al. 1991). Although the ratio is larger than unity at some positions, it can be understood as a case with a temperature gradient at most positions. The $1 - 0 S(1)$ emission at $1'' - 1.''2$ south of the S nucleus shows slightly enhanced ratio of T_{vib} to T_{rot} although it is still consistent within errors with the thermal excitation with a temperature gradient. However, because the depression of the $2 - 1 S(3)$ emission is also observed as well as the enhanced $1 - 0 S(1)$ emission, UV fluorescent might contribute the H_2 emission to some extent there.

4. Discussion

4.1. Superwind origin of the H₂ emission

We find the three velocity components in the H₂ emission in the southern region of NGC 6240: 1) the blueshifted component (≈ -250 km s⁻¹ with respect to V_{sys}) which is recognized as a distinct C-shape distortion of the velocity field, 2) the high-velocity “wing” component (~ -1000 km s⁻¹ with respect to V_{sys}), and 3) the component indicating possible line splitting of ~ 500 km s⁻¹. In the following sections we focus on these kinematic properties and discuss the origin of the extremely intense H₂ emission of NGC 6240 in the course of a “superwind” hypothesis.

4.1.1. Evidence for superwind

First we discuss the origin of the high-velocity “wing” component (-1000 km s⁻¹ with respect to V_{sys}). It is difficult for the galaxy-galaxy collision at a speed of $75 - 200$ km s⁻¹ (van der Werf et al. 1993) to produce a high-velocity material at a speed up to ~ 1000 km s⁻¹ (van der Werf et al. 1993). Moreover, such a component is only found around the S nucleus and the southern region, not around the region between the two nuclei where the two galaxies are likely to collide with each other. Thus, the galaxy-galaxy collision would not be responsible for this component. On the other hand, superwind origin of such a high-velocity material is promising since broad optical emission lines are detected around nuclear 1 kpc region in this galaxy and is attributed to the superwind on the basis of morphological, kinematic, and spectral evidence (Heckman et al. 1990).

The possible line splitting seen in the southern region can also be attributed to the superwind activity. Such type of the velocity field is often observed in the region of the expanding shell-like structure or biconical outflow seen in most superwind galaxies (e.g., Heckman et al. 1990). Most previous authors noted the extended south-south-west component $1'' - 2''$ away from the S nucleus (Elston & Maloney 1990; Herbst et al. 1990; van der Werf et al. 1993). Because this region is located at another side of the interface between the two colliding galaxies and no energy source is detected such as a star-formation activity there, superwind activity would be a most plausible agent for exciting the molecular gas in this region. The region showing line splitting corresponds spatially to this component, suggesting that a superwind indeed affects the molecular gas at this region. Slight blueshift in this region (-100 km s⁻¹) can be understood if we assume that the expanding direction of the bubble is not within the sky plane but is slightly tilted to our line-of-sight. It is interesting that the CO emission also extends toward this direction and

shows broader emission line profile like $1 - 0$ $S(1)$ emission (Tacconi et al. 1999), indicating that both of the cold (traced by CO) and the warm (traced by $1 - 0$ $S(1)$) molecular gas is affected by the superwind activity.

The C-shaped velocity field around the S nucleus strongly support the idea that the H_2 emitting gas is affected by the superwind activity. There are some nearby examples showing cold gas (atomic and molecular gas) outflow at a speed of several hundred $km\ s^{-1}$ (e.g., Phillips 1993; Nakai et al. 1987; Ohyama & Taniguchi 1997). Theoretical calculations also predict such an expanding structure (e.g., Suchkov et al. 1994). It is expected that some of the gas entrained in the high-velocity ionized gas outflow would be heated up by the shock to form a shell with the intense H_2 emission. If there is an expanding shell around the S nucleus, the redshifted component would be obscured by the heavy dust extinction around the S nucleus. As noted before, the dust extinction is severe even in K band ($A_k \gtrsim 22$ mag), which is dusty enough to obscure the H_2 emission from behind the nucleus and only blueshifted velocity structure is expected to be observed⁵, i.e., the velocity field would be C-shaped. This type of a velocity structure is one of the common characteristics seen in galaxies with superwinds (e.g., Heckman et al. 1990).

Since it is well known that this galaxy actually exhibits a superwind activity (e.g., Heckman et al. 1987, 1990; Armus et al. 1990; Keel 1990), it is natural to attribute these three velocity components to the entrained and shocked molecular gas within the superwind. Because both of the high-velocity wing component and the line splitting is not detected around the N nucleus, the starburst and the superwind of the S nucleus would be responsible for exciting these components. This interpretation is supported by the fact that the $[Fe\ II]\lambda 1.64\mu m$ emission, which is considered to arise at a shock driven by supernova explosions (van der Werf et al. 1993; Sugai et al. 1997), is much stronger at the S nucleus than at the N nucleus. All these considerations lead us to conclude that most H_2 emission in the southern region comes from the H_2 gas entrained in and shocked by the superwind blowing from the S nucleus.

Recently, Tacconi et al. (1999) conducted a high-resolution $^{12}CO(J = 2 - 1)$ mapping. They found a velocity gradient along the position angle of $\sim 45^\circ$ and showed the presence of blueshifted ($\sim -350\ km\ s^{-1}$ with respect to their $V_{sys} = 7320\ km\ s^{-1}$) molecular gas around the S nucleus. The trend of this gradient is similar to that found in the $1 - 0$ $S(1)$ emission (van der Werf et al. 1993). The peak position of the blueshifted CO emission ($V_\bullet = 6805 - 7005\ km\ s^{-1}$) is located at just $\sim 0.^{\prime\prime}2$ north of the S nucleus, indicating the presence of the blueshifted

⁵ Although the peak position of the molecular gas is located around $0.^{\prime\prime}6$ north of the S nucleus, significant fraction of the gas is distributed around the S nucleus (Tacconi et al. 1999). We expect that the column density around the S nucleus is still enough to obscure the redshifted part of the H_2 emission.

cold molecular gas around the S nucleus. Thus, it is very likely that some part of the cold molecular gas traced with the CO emission is heated up by the shock driven by the superwind to emit blueshifted $1 - 0$ $S(1)$ emission around the S nucleus.

4.1.2. Evidence against galaxy-galaxy collision

In spite of many pieces of evidence for the superwind origin of the H_2 emission, we find no evidence for the galaxy-galaxy collision origin of the strong $1 - 0$ $S(1)$ emission. In the collision model, kinetic energy released by the global collision of the two nuclei is converted to $1 - 0$ $S(1)$ emission. Thus, most intense $1 - 0$ $S(1)$ emission is expected to arise from the collision interface. We, however, find that the peak of the emission is located much closer to the S nucleus, being inconsistent with the model prediction. In addition to the discussion on the flux distribution, the kinematic information gives another clue against the collision model. We find a C-shaped velocity distortion of the H_2 emission at a maximum blueshifted velocity of -250 $km\ s^{-1}$ around the S nucleus. On the other hand, the stellar velocity difference between the two nuclei is less than 75 $km\ s^{-1}$ (Lester & Gaffney 1994), indicating that only emission line component is blueshifted around the S nucleus⁶. Thus, any models in which the H_2 emission is associated with the stellar component of the S nucleus can be rejected. Moreover, although some kind of a violent dynamical structure is expected at the interface of the two nuclei in the collision model, such as a sudden velocity change and/or a large velocity dispersion, such evidence is found neither around the region between the two nuclei where two galaxies are likely to be colliding nor other regions along the slit. In spite of these difficulties in the collision model, a superwind model can easily explain the velocity field, i.e., an expanding shell-like structure whose redshifted part is obscured by the heavy dust extinction on the extended H_2 gas with a nearly flat velocity field. Hence, we argue that the galaxy-galaxy collision would not be a main agent of the strong $1 - 0$ $S(1)$ emission of NGC 6240. Note, however, that we cannot reject a possibility of the galaxy-galaxy collision model since all pieces of evidence described above are not direct ones.

⁶ The stellar heliocentric velocity reported by Lester & Gaffney (1994) is $V_\odot = 7275 \pm 50$ $km\ s^{-1}$ and is consistent with the H_2 emission velocity measured around the N nucleus. We thus confirm that the emission line component around the S nucleus is blueshifted with respect to the stellar one.

4.1.3. Spatial and dynamical structure of the superwind

Theoretical calculations predict that a superbubble is formed at the early stage of the superwind evolution and that it will break out to form a biconical structure when the bubble extends large enough compared with the scaleheight of the surrounding material (Tomisaka & Ikeuchi 1988; Heckman et al. 1990; Suchkov et al. 1994). The superbubble is originally spherical around the starburst nucleus and will elongate into the direction where the density gradient is the largest (Tomisaka & Ikeuchi 1988; Suchkov et al. 1994). This direction is usually perpendicular to the dense disk gas in case of the normal nuclear starburst in spiral galaxies. In the case of NGC 6240, however, this would not be the case since the surrounding matter is expected to be highly disturbed in the course of the merging process, leading to the complicated superwind structure as observed (e.g., Heckman et al. 1987; Armus et al. 1990; Keel 1990). Thus, it is important to discuss the superwind morphology and the velocity structure in detail in order to know the distribution of the ambient matter and to understand how the superwind interacts with this gas.

As pointed out before, the emission line structure is not symmetric around the S nucleus. Rather, the emission is extended farther to the south of the S nucleus ($\sim 3''$, or 1.4 kpc) than to the north ($\sim 1''$, or 450 pc). At the south region, we find a kinematic evidence for the expanding structure (i.e., the high-velocity wing component and the line splitting). It is difficult to say clearly whether the southern region shows a closed bubble-like structure or an open conical structure because of the low surface intensity of the $1 - 0$ $S(1)$ emission. At the north of the S nucleus, the emission line velocity goes back to V_{sys} at just $\sim 1''$ north of the S nucleus. A compact expanding bubble can explain such a property in which the bubble is expanding to the north in the sky plane and the line-of-sight expanding velocity becomes to be zero at the top of the bubble. Hence, a highly asymmetric elongated bubble/wind expanding to north-south direction within the sky plane would be a most likely picture of the superwind of NGC 6240.

Here we compare the observed size and velocity of the bubble with that of the theoretical expectations. Following Heckman et al. (1996), we assume an idealized model of a single spherical bubble within the uniform surrounding medium (n_0). The kinetic energy (L_{mech}) is assumed to be injected at a constant rate during a time (t) and the radiative losses are negligible. In this case, the radius (r) and the expanding velocity (v) can be expressed as

$$L_{\text{mech}} = 8 \times 10^{42} L_{\text{bol},11} \text{ ergs s}^{-1}, \quad (1)$$

$$r = 7L_{\text{mech},43}^{1/5} n_{0,-2}^{-1/5} t_7^{3/5} \text{ kpc}, \quad (2)$$

$$v = 410 L_{\text{mech},43}^{1/5} n_{0,-2}^{-1/5} t_7^{-2/5} \text{ km s}^{-1}, \quad (3)$$

where $L_{\text{mech},43}$ is the kinetic energy injection rate in units of 10^{43} ergs s^{-1} , $L_{\text{bol},11}$ is the bolometric luminosity in units of $10^{11} L_{\odot}$, $n_{0,-2}$ is the number density of the ambient gas in units of 10^{-2} cm^{-3} , and t_7 is the time in units of 10^7 years (Heckman et al. 1993, 1996). The time (t) is estimated as $r_{\text{bubble}}/v_{\text{expansion}} \simeq 500 \text{ pc} / 250 \text{ km s}^{-1} \simeq 2 \times 10^6$ years, indicating relatively young age of the bubble (see for other examples of the young superwind; Yoshida, Taniguchi, & Murayama 1999 and references therein). The bolometric luminosity is taken from Wright et al. (1984) and is $L_{\text{bol}} = 5.0 \times 10^{11} L_{\odot}$ (converted to our adopted distance). Substituting these values into the equations, we estimate that $r = 3.5, 2.2, 1.4, 0.88, 0.56 \text{ kpc}$ and $v = 1030, 650, 410, 260, 160 \text{ km s}^{-1}$ for $n_0 = 10^{-2}, 10^{-1}, 10^0, 10^1, 10^2 \text{ cm}^{-3}$, respectively. Comparing with the observation, we find that the observation can be well represented (within a factor of two) by the model with $n_0 = 10^{1-2} \text{ cm}^{-3}$. Although the inferred density is higher than that of the usual extragalactic ambient matter ($\sim 10^{-2} \text{ cm}^{-3}$), it can be a natural consequence of the smaller size of the bubble ($r \simeq 500 \text{ pc}$) compared with the total size of the entire galaxy ($r \simeq 30 \text{ kpc}$: Heckman et al. 1987). The asymmetric structure of the bubble can be understood as a result of the density gradient of the ambient matter, i.e., smaller radius toward north direction where the ambient gas density is higher and vice versa. This result is consistent with the fact that the CO is concentrated toward north direction of the S nucleus. In this way, the superbubble model can reproduce the observed properties very well. It is interesting to point out that the age of the bubble ($\sim 2 \times 10^6$ years) is much younger than that of Arp 220 ($\sim 3 \times 10^7$ years: Heckman et al. 1996).

Previous narrow-band H_2 imaging studies have revealed an extended complex H_2 emission-line structure around the two nuclei (Herbst et al. 1990; van der Werf et al. 1993; Sugai et al. 1997) and it is very difficult to imagine a simple bubble-like structure in them. Optical narrow-band imaging studies also show extended ($\sim 60 \times 50 \text{ kpc}$: Heckman et al. 1987) filamentary emission-line nebula (see also Armus et al. 1990; Keel 1990). Inhomogeneity of the surrounding material would be a main reason for these complex structures. However, we point out that two prominent tail-like features of the H_2 emission are extending toward southeast and southwest directions from the S nucleus. These structures are most clearly visible in an image of Sugai et al. (1997; see their Figure 1). If we assume that the tails imply the projected edges of a cone, the superwind seems to be blowing toward south with an opening angle of $\sim 90^\circ$. Further discussions on the detailed structure of the superwind would require deeper emission-line images.

It seems interesting to point out that the size of the bubble we find (~ 1 kpc) is much smaller than that of the large-scale optical nebula ($\sim 60 \times 50$ kpc) although both are likely to be driven by numerous supernova explosions in the nuclear region. In order to produce the large-scale nebula within the timescale for a small bubble ($\sim 2 \times 10^6$ years), unusually large expanding velocity (> 10000 km s $^{-1}$) is required. Thus, the superwind in this galaxy seems to comprise at least two bubbles/winds with different ages, i.e., the young compact bubble and the surrounding older larger bubble/wind, although the number of bubbles is not certain. The age of the larger bubble/wind is estimated to be 8×10^7 years under an assumption of the common expanding velocity for both the bubbles/winds (250 km s $^{-1}$). In order to make such a multiple bubble system, starburst events must have occurred twice, i.e., $\sim 2 \times 10^6$ years and $\sim 8 \times 10^7$ years ago. We expect that the starburst activity has been triggered by the tidal dynamical disturbance several times when the separation of the two nuclei becomes the smallest while they are orbiting around each other.

Theoretical models predict that an expanding bubble should brake out because of Rayleigh-Taylor instability when a bubble expands into an outer low density halo (Tomisaka & Ikeuchi 1988; Heckman et al. 1990; Suchkov et al. 1994). If the density of the ambient matter is high enough or the energy supply from the nuclear region is small enough, instability is suppressed and the ionized gas would be confined not to form a biconical structure. Since starburst activity in NGC 6240 is relatively high [$L(\text{IR}) = 4.6 \times 10^{11} L_\odot$], it is expected that the bubble would be broken out unless the density of the ambient matter is unusually high. However, NGC 6240 might be an unusual case with an extraordinary high density extragalactic matter. It is well known that the huge amount of the molecular gas is distributed between the two nuclei, rather than at each nucleus, as a result of the dynamical disturbance caused by the galaxy-galaxy merger (Bryant & Scoville 1999; Tacconi et al. 1999). If the molecular gas accumulates between the nuclei before the superbubble begins to expand (10^{7-8} years after the onset of the starburst), the expanding superbubble toward the north of the S nucleus would be blocked by this dense extranuclear molecular gas and the broken-out of the bubble would be inhibited, forming a compact bubble-like structure as observed. On the other hand, the superbubble would expand more freely to the south direction. If this is the case, we can explain the reason why the peak position of the $1 - 0$ $S(1)$ emission comes closer to the S nucleus than the peak position of the CO emission since the shock front between the bubble and the ambient matter should come between the two.

In this model, the H₂ emission in the northern region is difficult to be explained. Judging from a complex morphology and velocity field seen also in this region (van der Werf et al. 1993), we would argue that the most

plausible agent is a superwind. Starburst and/or AGN activities of the N nucleus, rather than that of the S nucleus, might be responsible for the superwind activity. In fact, the activity of the N nucleus is indicated by $[\text{Fe II}]\lambda 1.64\mu\text{m}$ emission associated with it (van der Werf et al. 1993). Since the superwind activity seems to have occurred at least twice, it seems also possible that the northern H_2 emission is excited by the shock driven by the older superwind, rather than by the current one which is responsible for the C-shaped velocity distortion around the S nucleus. We cannot discuss this possibility further only with our data.

4.1.4. Can superwind explain the huge H_2 luminosity?

Most previous authors discussed that the galaxy-galaxy collision is the main energy source of the intense H_2 emission in NGC 6240 because the starburst activity would not be strong enough to reproduce its huge H_2 luminosity [$L(1 - 0 \text{ S}(1)) \simeq 1 \times 10^8 L_\odot$; Rieke et al. 1985; Draine & Woods 1990; van der Werf et al. 1993]. However, one must remember that the previous estimates of the $1 - 0 \text{ S}(1)$ luminosity assume an ordinary nuclear starburst. We emphasize that such estimates would not be applicable to the case of NGC 6240 in which the superwind interacts with the dense intergalactic medium.

If we adopt a canonical value of the conversion factor of kinetic energy supplied from supernova explosions to H_2 emission (~ 0.02), required supernova rate is as high as 15 supernovae per year (Draine & Woods 1990). The supernova rate in NGC 6240 is estimated to be only $3.2 - 4.8$ if we simply scale up the supernova rate of the nearby prototypical starburst galaxy M82 ($\sim 0.2 - 0.3$ SNRs per year; Rieke et al. 1980; Kronberg, Biermann, & Schwab 1985) with their far-infrared luminosities [$L(\text{FIR}) = 3.3 \times 10^{10} L_\odot$ for M82 and $5.2 \times 10^{11} L_\odot$ for NGC 6240; Heckman et al. 1990]⁷. As pointed out by Draine & Woods (1993), however, the efficiency can be as large as 0.2 if the medium is clumpy and the cloud-crushing is efficient. If the cloud-intercloud density constant is $\simeq 10^2$, the cloud-crushing will produce shock waves in the clouds with a shock speed of $30 - 50 \text{ km s}^{-1}$ where $1 - 0 \text{ S}(1)$ emission is efficiently produced when the blastwave speed is $300 - 500 \text{ km s}^{-1}$ (Cowie, McKee, and Ostriker 1981; see also Elston & Maloney 1990). As noted before, NGC 6240 seems to be a rare case with a huge amount of the intergalactic matter. It is easy to imagine that this matter is disturbed and its spatial distribution becomes highly clumpy in the course of the merging process. It is important to remember that this galaxy shows unusually broad line width ($\sim 550 \text{ km s}^{-1}$

⁷ Based on the extensive modeling of the starburst properties of M82 and NGC 6240, Rieke et al. (1985) showed that the starburst models for the two galaxies are similar, suggesting that the supernova rate scales with the far-infrared luminosity between the two galaxies.

FWHM), suggesting that the cloud-crushing mechanism might be very efficient. We thus argue that the $1 - 0$ $S(1)$ luminosity can be explained only by the superwind activity.

Another key point in discussing the origin of the huge H_2 luminosity is its unusually large $1 - 0$ $S(1)/Br\gamma$ intensity ratio. The ratio is the largest one observed so far in LIGs (Goldader et al. 1995). Although the ratio has been reported to be as large as ~ 45 (van der Werf et al. 1990), we find the ratio to be only $\simeq 10$ around the S nucleus. The main reason for this discrepancy would be the data quality. The high signal-to-noise ratio, high spatial resolution spectra of ours enable us to measure the weak $Br\gamma$ feature more accurately than the previous works (Remember that $Br\gamma$ is detected only around the S and the N nuclei while peak of the H_2 emission is offset from the nuclei). Although this ratio ($\simeq 10$) is still very large, it can now be explained by normal star-formation models. Mouri & Taniguchi (1992) calculated the $1 - 0$ $S(1)/Br\gamma$ ratio for various starburst models and found that the ratio ranges 0.1 – 10. The ratio becomes larger in models with the lower upper mass limit of the initial mass function. This is because kinetic energy exciting H_2 released from supernova explosions does not change with the mass of their progenitors, while ionizing photons from O-type stars decrease rapidly with the decrease of the mass of the most massive stars. Also, the ratio becomes larger in models at a post-starburst phase because O-type stars supplying most ionizing photons are gone. Thus, the O-type star deficient stellar population can explain the observed ratio. In fact, some evidence for the O-type star deficient stellar population of this galaxy was found (Draine & Woods 1990; Tanaka et al. 1991). Note, however, that our result only indicates that the superwind-driven shock is enough to explain the H_2 luminosity and does not necessarily rule out the contribution of a global shock caused by the galaxy-galaxy collision.

Here one might have a question on why only NGC 6240 shows unusually strong H_2 emission. One of the possible reasons is that the chance probability for the superwind to interact with the extragalactic dense matter is very small. NGC 6240 should be a rare case in which the direction of the mass transfer during the merging process and that of the outflow of the superwind are nearly the same. Another possible reason is the short timescale of the H_2 emitting phase during the evolution of this galaxy. If the expansion velocity of the superbubble is ~ 250 km s $^{-1}$ as suggested by the maximum line-of-sight velocity of the C-shaped velocity distortion around the S nucleus, the shock front would pass through the core of the CO emission (~ 500 pc: Tacconi et al. 1999) in only $\sim 2 \times 10^6$ years. As pointed out before, the age of the bubble is also very young ($\sim 2 \times 10^6$ years). Because these timescales are significantly smaller than that of the starburst ($\sim 10^{7-8}$ years), the intense H_2 emission would fade out soon and only weaker H_2

emission associated with the nuclear star formation and/or AGN activities would be observed like other ordinary LIGs after $\gtrsim 2 \times 10^6$ years. It seems very likely that the coincidence of both two special conditions make NGC 6240 be a very rare object with an exceptionally strong H₂ emission.

4.2. Physical conditions of the H₂ gas

The excitation mechanism of the H₂ emission of NGC 6240 has long been a controversy. Based on a spectrum presented by Lester et al. (1988), several excitation mechanisms besides the thermal excitation have been proposed. Two important characteristics of the Lester et al.'s spectrum are 1) the rotation temperature is lower than the vibration temperature ($T_{\text{rot}} = 1300$ K and $T_{\text{vib}} = 2860$ K) and 2) 2 – 1 $S(3)$ emission is unusually weak and only upper limit is reported. Tanaka et al. (1991) discussed that the UV fluorescence mechanism is significant in order to explain the first characteristic. They pointed out that the reported upper limit of the 2 – 1 $S(3)$ flux is too small and they are not serious on the second characteristic. On the other hand, Draine & Woods (1990) emphasized the importance of the second characteristic and favored the X-ray heating mechanism. The formation pumping mechanism is also discussed in order to reproduce the peculiar spectrum (Mouri & Taniguchi 1995).

Recently, Sugai et al. (1997) presented their high quality H₂ spectrum. Surprisingly, their spectrum significantly differs from that of Lester et al. (1988) and can be interpreted as a pure thermal excitation because they found neither an excess of the vibration temperature nor weaker-than-expected 2 – 1 $S(3)$ emission ($T_{\text{rot}} \simeq T_{\text{vib}} = 1910$ K; Sugai et al. 1997). Why the two spectra are different from each other? One possible reason is the different aperture positions. Sugai et al. (1997) placed their slit at the midpoint of the two nuclei. At this region, our data indicates a thermal excitation, being consistent with Sugai's result. On the other hand, Lester et al. (1988) placed their aperture at "the position of peak signal" which can be interpreted that they placed their aperture closer to the S nucleus which is brighter than the N nucleus. One evidence suggesting the aperture difference is the equivalent width of the 1 – 0 $S(1)$ emission: Comparing with their spectra, we find that the equivalent width measured by Lester et al. (1988) is smaller than that of Sugai et al. (1997). Since the equivalent width changes dramatically with positions and it becomes smaller around the S nucleus (Figure 3), it seems very likely that Lester et al. (1988) indeed placed their aperture closer to the S nucleus. In fact, our spectrum at +0."46 north of the S nucleus, where the 1 – 0 $S(1)$ flux is the maximum with an equivalent width $\simeq 30 - 70$ Å, looks similar to the spectrum of Lester et al. (1988) that shows the 1 – 0 $S(1)$ equivalent width 62 Å. Our spectrum at +1."15 north of the S nucleus where

equivalent width is the maximum ($\simeq 100\text{\AA}$) looks similar to the spectrum of Sugai et al. (1977) (see Figures 2 and 3). Unfortunately, however, because of the smaller equivalent widths of emission lines and strong stellar absorption features, we cannot confirm the two characteristics of Lester et al.'s spectrum around the S nucleus. Because [Fe II] emission is detected at the S nucleus and supernova explosions are the most probable agents (van der Werf et al. 1993; see also Sugai et al. 1997), it is expected that the intense starburst around the S nucleus supplies huge amount of UV photons, leading to additional UV fluorescent excitation as well as the shock heating (Tanaka et al. 1991). The UV photons may also be responsible for a possible UV fluorescent excitation found at $\sim 0.^{\prime\prime}5$ south of the S nucleus.

We find no evidence for the X-ray heating (Draine & Woods 1990) since $2 - 1$ $S(3)$ is detected except around the S nucleus. Also we find no excitational evidence for the AGN activity anywhere. Thus, we conclude that the main excitation mechanism is the thermal excitation caused by the shock heating at most positions with a possible additional contributions of UV fluorescent and/or X-ray heating around the S nucleus.

5. Proposed Scenario of NGC 6240 System

Here we summarize a proposed scenario of the merging and superwind evolution in NGC 6240.

1) Two gas-rich galaxies (the N and the S nuclei) merge. A huge amount of molecular gas is forced to fall onto the two nuclei as a result of the dynamical disturbance during the merging process. At the same time, the dynamical disturbance triggers the nuclear starburst at each nucleus. The starburst activity is stronger at the S nucleus. A schematic picture at this stage is shown in Figure 9(a). The nuclear starburst activity was triggered several times while the two nuclei are orbiting around each other.

2) When 10^{7-8} years passed since the onset of the starburst, the massive stars begin to explode and a superbubble starts to expand. As the superbubble expands, it interacts with the dense and perturbed molecular gas at the northern region of the S nucleus and heats it up. Stronger-than-normal H_2 emission lines are observed there as a result of the efficient cloud-crushing mechanism. Both the molecular gas that was supplied during the merging process and the material blown-off by the superwind would emit strong H_2 emission lines. At the same time, the bubble expands more freely toward the south direction and forms an asymmetrically elongated superbubble. A schematic picture at this stage is shown in Figure 9(b). Multiple bubbles are formed as a result of multiple triggerings of the starburst.

3) The strong H₂ emission would be observed only for 2×10^6 years in which the expanding superbubble interacts with the extragalactic dense matter. Then NGC 6240 would be observed as a normal LIGs with a moderate H₂ emission.

6. Summary

We have performed spatially-resolved spectroscopic analyses of the H₂ emission lines in NGC 6240. We find that most of the H₂ emission is attributed to the shock driven by the superwind of the S nucleus, rather than by the conventional global shock driven by the collision of the two nuclei. Our main conclusions are listed below.

- 1) The peak position of the H₂ 1 – 0 *S*(1) emission is not at the midpoint of the two nuclei. Rather, it is located much closer to the S nucleus.
- 2) In the southern region (the region around the S nucleus and south of the nucleus) we identify the following three velocity components in the H₂ emission: a) the blueshifted shell component (≈ -250 km s⁻¹ with respect to V_{sys}) which shows a distinct C-shape distortion in the velocity field around the southern nucleus, b) the high-velocity blueshifted “wing” component (~ -1000 km s⁻¹ with respect to V_{sys}), and c) the component indicating possible line splitting of ~ 500 km s⁻¹. The latter two components extend to the south from the S nucleus.
- 3) The presence of these three velocity components can be explained naturally by the superwind activity of the S nucleus. On the other hand, we found no evidence for the classical galaxy-galaxy collision origin of the 1 – 0 *S*(1) emission, although we cannot reject the possibility completely.
- 4) The huge 1 – 0 *S*(1) luminosity can be explained only by the superwind-driven shock heating, if we assume a higher conversion efficiency of the kinetic energy of SNRs to the 1 – 0 *S*(1) emission through the efficient cloud-crushing mechanism. This mechanism efficiently works at the shock interface between the expanding superbubble and the extranuclear molecular gas since the molecular gas is likely to be highly clumpy and is dynamically disturbed during the merging of the two nuclei.
- 5) The excitation condition of the H₂ emission lines is the shock heating at most positions except for around the S nucleus where additional UV fluorescent excitation is expected.
- 6) We propose an evolutional scenario of NGC 6240 in which the galaxy-galaxy merger drives the molecular gas to accumulate between the two nuclei and triggers a starburst activity at each nucleus. The intense 1 – 0 *S*(1) emission comes from the molecular gas entrained in and shocked by the superwind which starts to blow 10^{7-8} after years

since the onset of the starburst.

We would like to thank all the people in the Subaru project. This research has been done using the facilities at the Astronomical Data Analysis Center of the National Astronomical Observatory, Japan, which is an inter-university research institute of astronomy operated by Ministry of Education, Science, Culture, and Sports.

References

Armus, L., Heckman, T.M., Miley, G.K. 1990, *ApJ* 364, 471

Baan, W.A., Haschick, A.D., Buckley, D., Schmelz, J.T. 1985, *ApJ* 293, 394

Beckwith, S., Evans, N.J., II, Gatley, I., Gull, G., Russell, R.W. 1983, *ApJ* 264, 152

Binney, J., Merrifield, M. 1998, *Galactic Astronomy*, Princeton Series in Astrophysics (Princeton, New Jersey)

Bryant, P.M., Scoville, N.Z. 1999, *ApJ* 117, 2632

Colbert, E.J.M., Wilson, A.S., Bland-Hawthorn, J. 1994, *ApJ* 436, 89

Condon, J.J., Condon, M.A., Gisler, G., Puschell, J.J. 1982, *ApJ* 252, 102

Cowie, L.L., McKee, C.F., Ostriker, J.P. 1981, *ApJ* 247, 908

DePoy, D.K., Becklin, E.E., Wynn-Williams, C.G. 1986, *ApJ* 307, 116

Doyon, R., Wells, M., Wright, G.S., Joseph, R.D., Nadeau, D., James, P.A. 1994, *ApJL* 437, 23

Draine, B.T., Woods, D.T. 1990, *ApJ* 363, 464

Eales, S.A., Becklin, E.E., Hodapp, K.-W., Simons, D.A., Wynn-Williams, C.G. 1990, *ApJ* 365, 478

Elston, R., Maloney, P. 1990, *ApJ* 357, 91

Fried, J.W., Schulz, H. 1983, *A&A* 118, 166

Garwood, R.W., Helou, G., Dickey, J.M. 1987, *ApJ* 322, 88

Goldader, J.D., Joseph, R.D., Doyon, R., Sanders, D.B. 1995, *ApJ* 444, 97

Heckman, T.M., Balick, B., van Breugel, W.J.M., Miley, G.K. 1983, *AJ* 88, 583

Heckman, T.M., Armus, L., Miley, G.K. 1987, *AJ* 92, 276

Heckman, T.M., Armus, L., Miley, G.K. 1990, *ApJS* 74, 833

Heckman, T.M., Lehnert, M.D., Armus, L. 1993, in *The Environment and Evolution of Galaxies*, ed J.M. Shull, H.A. Thronson Jr. (Kluwer, Netherlands) p455

Heckman, T.M., Dahlem, M., Eales, S.A., Fabbiano, G., Weaver, K. 1996, *ApJ* 457, 616

Herbst, T.M., Graham, J.R., Beckwith, S., Tsutsui, K., Soifer, B.T., Matthews, K. 1990, *AJ* 99, 1773

Iwasawa, K., Comastri, A. 1998, *MNRAS* 297, 1219

Joseph, R.D., Wright, G.S. 1985, *MNRAS* 214, 87

Kaifu, N. 1998, *SPIE* 3352, 14

Keel, W.C. 1990, AJ 100, 356

Klaas, U., Hass, M., Heinrichsen, I., Schulz, B. 1997, A&A 325, L21

Kronberg, D.P., Biermann, P., Schwab, F.R. 1985, ApJ 291, 693

Lester, D.F., Gaffney, N.I. 1994, ApJL 431, 13

Lester, D.F., Harvey, P.M., Carr, J. 1988, ApJ 329, 641

Moorwood, A.F.M., Oliva, E. 1990, A&A 239, 78

Motohara, K., Maihara, T., Iwamuro, F., Oya, S., Imanishi, M., Terada, H., Goto, M., Iwai, J. et al. 1998, SPIE 3354, 659

Mouri, H. 1994, ApJ 427, 777

Mouri, H., Taniguchi, Y. 1992, ApJ 386, 68

Mouri, H., Taniguchi, Y. 1995, ApJ 449, 134

Mouri, H., Taniguchi, Y., Kawara, K., Nishida, M. 1989, ApJL 346, 73

Nakai, N., Hayashi, M., Handa, T., Sofue, Y., Hasegawa, T., Sasaki M. 1987, PASJ 39, 685

Ohyama, Y., Taniguchi, Y. 1998, ApJL 499, 934

Osterbrock, D.E. 1989, *Astrophysics of Gaseous Nebulae and Active Galactic Nuclei* (Mill Valley, California)

Phillips, A.C. 1993, AJ 105, 486

Rieke, G.H., Lebofsky, M.J., Thompson, R.I., Low, F.J., Tokunaga, A.T. 1980, ApJ 238, 24

Rieke, G.H., Cutri, R.M., Black, J.H., Kailey, W.F., McAlary, C.W., Lebofsky, M.J., Elston, R. 1985, ApJ 290, 116

Sanders, D.B., Mirabel, I.F. 1985, ApJL 298, 31

Sanders, D.B., Mirabel, I.F. 1996, ARA&A 34, 749

Smith, C.H., Aitken, D.K., Roche, P.F. 1989, MNRAS 241, 425

Solomon, P.M., Downes, D., Radford, S.J.E., Barrett, J.W. 1997, ApJ 478, 144

Suchkov, A.A., Balsara, D.S., Heckman, T.M., Leitherer, C. 1994, ApJ 430, 511

Sugai, H., Malkan, M.A., Ward, M.J., Davies, R.I., McLean, I.S. 1997, ApJ 481, 186

Tanaka, M., Hasegawa, T., Gatley, I. 1991, ApJ 374, 516

Tanaka, M., Hasegawa, T., Hayashi, S.S., Brand, P.W.J.L., Gatley, I. 1989, ApJ 336, 207

Tacconi, L.J., Genzel, R., Tecza, M., Gallimore, J.F., Downes, D., Scoville, N.Z. 1999, astro-ph/9905031

Thronson, H.A. Jr, Majewski, S., Descartes, L., Hereld, M. 1990, ApJ 364, 456

Table 1. Previous measurements of systemic velocity of NGC 6240.

| V_{\bullet} (km s $^{-1}$) | Waveband | Comments | Reference |
|-------------------------------|-----------------------------|---|---------------------------------|
| 7287 | HI 21 cm | Absorption, Single dish | Garwood, Helou, & Dickey (1987) |
| 7350 \pm 65 | HI 21 cm | Absorption, Single dish | Heckman et al. (1983) |
| 7270 | HI 21 cm | Absorption, Single dish | Baan et al. (1985) |
| 7253 | OH 1667, 1667 MHz | Absorption, Single dish | Baan et al. (1985) |
| 7285 | $^{12}\text{CO}(J = 1 - 0)$ | Single dish observation | Sanders & Mirabel (1985) |
| 7298 | $^{12}\text{CO}(J = 1 - 0)$ | Single dish | Solomon et al. (1997) |
| 7335 \pm 13 | $^{12}\text{CO}(J = 1 - 0)$ | Interferometer | Bryant & Scoville (1999) |
| 7313 | $^{12}\text{CO}(J = 1 - 0)$ | Interferometer | Wang et al. (1991) |
| 7297 | 1 – 0 $S(1)$ | Estimated from van der Werf et al.'s figure 3 | van der Werf et al. (1993) |
| 7275 \pm 50 | Stellar CO absorption | K band | Lester & Gaffney (1994) |
| 7473 \pm 30 | Stellar CO absorption | K band | Doyon et al. (1994) |

Tomisaka, K., Ikeuchi, S. 1988, ApJ 330, 695

van der Werf, P.P., Genzel, R., Krabbe, A., Blietz, M., Lutz, D., Drapatz, B., Ward, M.J., Forbes, D.A. 1993, ApJ 405, 522

Wang, Z., Scoville, N.Z., Sanders, D.B. 1991, ApJ 368, 112

Wright, G.S., Joseph, R.D., Meikle, W.P.S. 1984, Nature 309, 430

Yoshida, M., Taniguchi, Y., Murayama, T. 1999, AJ 117, 1158

Figure Captions

Fig. 1. The K band image of NGC 6240. This image was obtained through a wide $2''$ slit with its position angle of 19° and is averaged over 2 pixels ($0.''23$). No correction for the dark subtraction and the flatfielding were applied since this image is taken just for the source acquisition. The coordinates are shown relative to the S nucleus in units of arcsecond. The spatial resolution is indicated with a circle at the lower left corner. Two white vertical lines indicate the slit position used for the spectroscopy ($0.''5$ width). The peak position of $^{12}\text{CO}(J = 2 - 1)$ (Tacconi et al. 1999) is marked with a cross sign. This position is corrected for $0.''15$ offset between the radio and the K band nuclei (see the main text for the detail).

Fig. 2. Spectra extracted over 2 pixels ($0.''23$) at various positions along the slit with the line identifications. Relative offset from the S nucleus are indicated at each spectrum in units of arcsecond as well as the positions of the N and the S nuclei. All spectra are normalized with the peak flux of the $1 - 0 S(1)$ emission. Zero flux levels are shifted for clarity and are indicated at the left ordinate for each spectrum. Some data points are removed since they are affected by bad pixels.

Fig. 3. $1 - 0 S(1)$ flux and velocity field along the slit. Positions of the N and the S nuclei are indicated at the top of the panels. 1σ errors are shown for the all plots. (*top*) $1 - 0 S(1)$ flux, continuum flux at $2.2\mu\text{m}$, and equivalent width of $1 - 0 S(1)$ (right ordinate) are shown with squares, circles, and crosses, respectively. (*middle*) Heliocentric velocity of the $1 - 0 S(1)$ emission measured with a single Gaussian function. (*bottom*) Line width (FWHM) of the $1 - 0 S(1)$ emission measured with a single Gaussian function.

Fig. 4. Velocity field of the $1 - 0 S(1)$ emission. Middle image shows a spectroscopic image of $1 - 0 S(1)$. In order to show the velocity structure clearly, the image is processed in the following ways. First, the continuum flux is removed by interpolating the adjacent continuum. Then, the peak of the resultant emission-line spectroscopic image is normalized to be unity at every row. Note that the contour levels shown in this image represent neither the relative flux level nor the significance of the flux as a result of the peak normalization. You can find the significance of the contour levels with the plots of the continuum and $1 - 0 S(1)$ flux in the left panel. The emission-line profile of the $1 - 0 S(1)$ emission at three representative positions (at three horizontal bars in the image marked as a, b, and c) are shown in the right panels. Typical errors of the profiles are indicated with vertical bars in each panel.

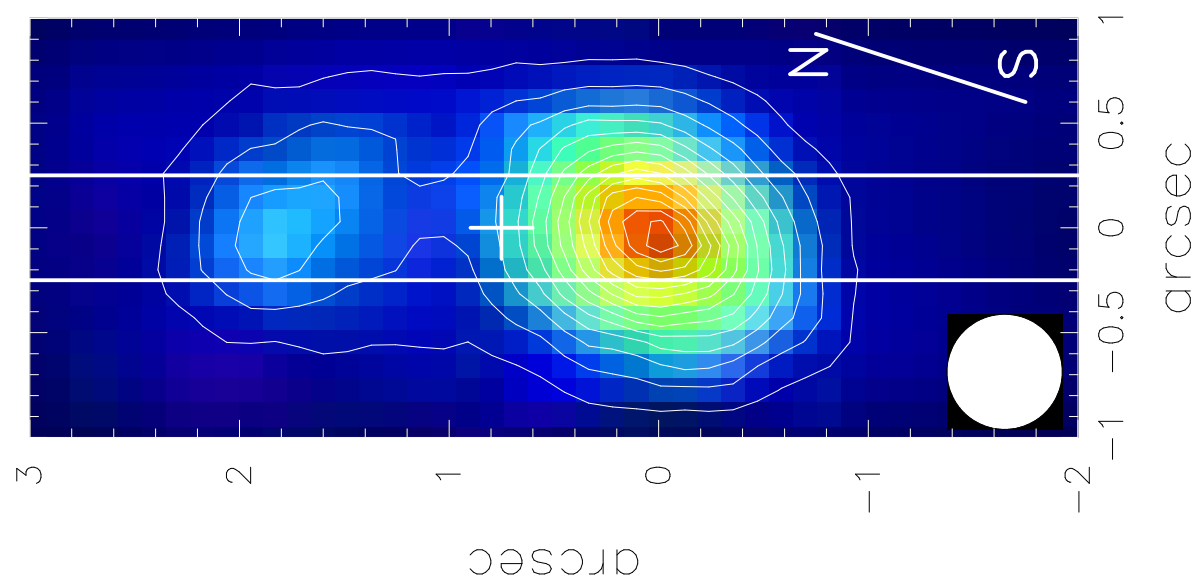
Fig. 5. The observed line profile of the $1 - 0 S(1)$ emission at $7''$ south of the S nucleus is compared with the model line profile. The continuum emission is removed for the observed profile. The blueshifted and redshifted model components are shown with a dotted and a short-dashed lines, respectively, and the sum of the two components is plotted with a long-dashed line. See the main text for the model description.

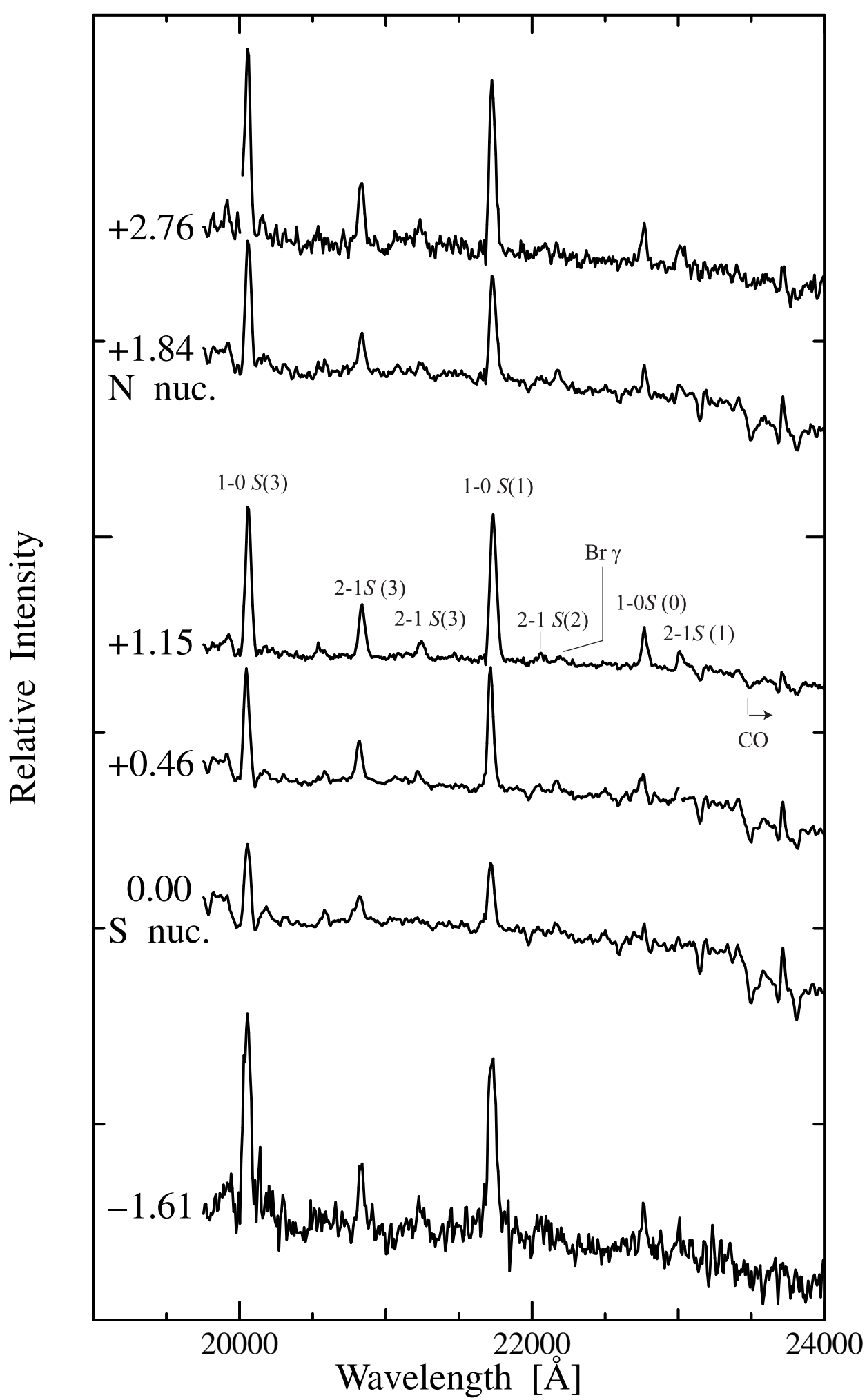
Fig. 6. The line ratio vs. line ratio diagram. $1 - 0 S(2)/1 - 0 S(0)$ ratio is plotted against $2 - 1 S(1)/1 - 0 S(1)$ ratio with 1σ errors. The locus shows the theoretical line ratios of the thermal excitation with the temperature < 3000 K (marked along the curve). Two open squares are observed data points for supernova remnants IC 443 and RCW 103 taken from Mouri (1994).

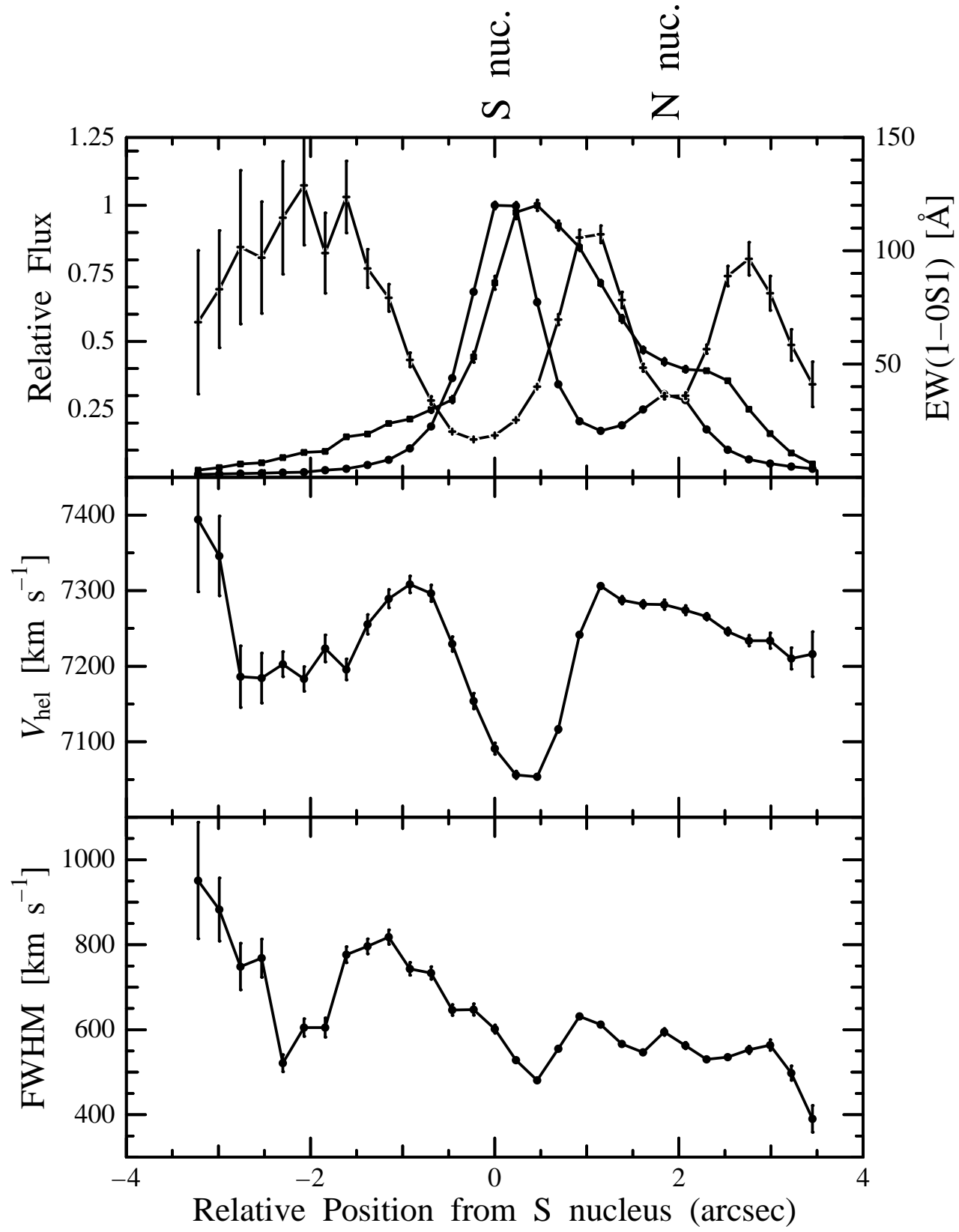
Fig. 7. The population diagrams. Populations relative to $(J, v)=(3, 1)$ state are plotted for $(2, 1)$, $(4, 1)$, $(3, 2)$, and $(5, 2)$ (corresponding to $1 - 0 S(0)$, $1 - 0 S(2)$, $2 - 1 S(1)$, and $2 - 1 S(3)$ emission lines, respectively) at every $0.^{\prime\prime}23$ with 1σ errors. Each diagram is shifted for clarity and the diagrams at the most southern and northern regions are plotted at the upper left and the lower right corners of the plots. Positions of the N and the S nuclei are indicated. Only lower limits of the populations of $(2, 1)$ state are measured around the S nucleus because of the weak $1 - 0 S(0)$ emission on the strong continuum emission with absorption lines.

Fig. 8. Spatial variation of the $v = 2 - 1$ vibration temperature (T_{vib}) and $v = 1$ rotation temperature (T_{rot}). 1σ errors are shown for the all plots. Positions of the N and the S nuclei are indicated. (top) The ratio of $T_{\text{vib}}/T_{\text{rot}}$ is plotted along the slit. The two dotted horizontal lines at 1 and 1.25 indicate the range expected for the thermal excitation (see the main text for the detail). (middle) The $2 - 1 S(1)/1 - 0 S(1)$ flux ratio (left ordinate) and T_{vib} (right ordinate) are shown along the slit. (bottom) The $1 - 0 S(2)/1 - 0 S(0)$ flux ratio (left ordinate) and T_{rot} (right ordinate) are shown along the slit.

Fig. 9. Our proposed scenario of NGC 6240 is schematically shown. (a) Schematic picture at the early stage of the merging with nuclear starburst and molecular gas transfer. See the main text for the detail. (b) Schematic picture at the late stage of the merging with the superwind and the intense H_2 emission. See the main text for the detail.







Continuum-subtracted
Peak-flux-normalized
Long Slit 1-0S(1) Image

